Highly Efficient Orange and Green Solid-State Light-Emitting Electrochemical Cells Based on Cationic IrIII Complexes with Enhanced Steric Hindrance

ARTICLE *in* ADVANCED FUNCTIONAL MATERIALS · APRIL 2007

Impact Factor: 11.81 · DOI: 10.1002/adfm.200600372

9 AUTHORS, INCLUDING:

Fei-Hu Chen
Anhui Medical University
131 PUBLICATIONS **2,115** CITATIONS
SEE PROFILE

Ken-Tsung Wong
National Taiwan University
261 PUBLICATIONS **8,072** CITATIONS
SEE PROFILE

ADVANCED FUNCTIONAL MATERIALS

FULL PAPER

DOI: 10.1002/adfm.200600372

Highly Efficient Orange and Green Solid-State Light-Emitting Electrochemical Cells Based on Cationic Ir^{III} Complexes with Enhanced Steric Hindrance**

By *Hai-Ching Su*, *Fu-Chuan Fang*, *Tsyr-Yuan Hwu*, *Hsing-Hung Hsieh*, *Hsiao-Fan Chen*, *Gene-Hsiang Lee*, *Shie-Ming Peng*, *Ken-Tsung Wong*,* and *Chung-Chih Wu**

Highly efficient orange and green emission from single-layered solid-state light-emitting electrochemical cells based on cationic transition-metal complexes $[Ir(ppy)_2sb]PF_6$ and $[Ir(dFppy)_2sb]PF_6$ (where ppy is 2-phenylpyridine, dFppy is 2-(2,4-difluorophenyl)pyridine, and sb is 4,5-diaza-9,9′-spirobifluorene) is reported. Photoluminescence measurements show highly retained quantum yields for $[Ir(ppy)_2sb]PF_6$ and $[Ir(dFppy)_2$ $sb]PF_6$ in neat films (compared with quantum yields of these complexes dispersed in *m*-bis(*N*-carbazolyl)benzene films). The spiroconfigured sb ligands effectively enhance the steric hindrance of the complexes and reduce the self-quenching effect. The devices that use single-layered neat films of $[Ir(ppy)_2sb]PF_6$ and $[Ir(dFppy)_2sb]PF_6$ achieve high peak external quantum efficiencies and power efficiencies of 7.1 % and 22.6 lm W^{-1}) at 2.5 V, and 7.1 % and 26.2 lm W^{-1} at 2.8 V, respectively. These efficiencies are among the highest reported for solid-state light-emitting electrochemical cells, and indicate that cationic transition-metal complexes containing ligands with good steric hindrance are excellent candidates for highly efficient solid-state electrochemical cells.

1. Introduction

Light-emitting electrochemical cells (LECs) possess several advantages over conventional organic light-emitting diodes (OLEDs). OLEDs typically require sophisticated multilayer structures and low-work-function cathodes to achieve high efficiencies and low operating voltages, while LECs generally require only a single emissive layer, which can be easily processed from solutions, and can conveniently use air-stable electrodes. The emissive layer of LECs contains mobile ions, which can drift toward electrodes under an applied bias. The spatially separated ions induce doping (oxidation and reduction) of the emissive materials near the electrodes, i.e., p-type doping near the anode and n-type doping near the cathode.[1] The doped regions induce ohmic contacts with the electrodes, and consequently facilitate the injection of both holes and electrons that recombine at the junction between p-type and n-type regions. As a result, a single-layered LEC device can be operated at very low voltages (close to E_g/e, where E_g is the energy gap of the emissive material and e is the elementary charge, 1.602×10^{-19} C) with balanced carrier injection, giving high power efficiencies. Furthermore, air-stable metals (e.g., Au and Ag) can be used because carrier injection in LECs is relatively insensitive to the work functions of the electrodes.

A polymer blend sandwiched between two electrodes comprised the first solid-state LEC device.[1] The polymer blend was composed of an emissive conjugated polymer, a lithium salt (lithium trifluoromethane sulfonate), and an ion-conducting polymer (poly(ethylene oxide); PEO). The salt provided mobile ions, and the ion-conducting polymer prevented the blend film from phase separation, the induction of which could result from polarity discrepancies between the conjugated polymer and the lithium salt. More recently, cationic transition-metal complexes have also been used in LECs, and show several advantages over conventional polymer LECs.[2–14] In such devices, no ion-conducting material is needed because the metal complexes are intrinsically ionic. In general, they show good thermal stabilities and charge-transport properties. Furthermore, high electroluminescence (EL) efficiencies can be expected because of the phosphorescent nature of the metal complexes. The first solid-state LEC based on transition-metal complexes, in which a ruthenium polypyridyl complex was utilized as the emissive material, was reported in 1996.[3] Since then, many efforts have been made to improve the performance characteristics of such LECs. In 1999, LECs based on

[*] Prof. C.-C. Wu, H.-C. Su, H.-H. Hsieh
Department of Electrical Engineering, Graduate Institute of Electro-optical Engineering and Graduate Institute of Electronics Engineering
National Taiwan University
Taipei 106 (Taiwan)
E-mail: chungwu@cc.ee.ntu.edu.tw
Prof. K.-T. Wong, F.-C. Fang, T.-Y. Hwu, H.-F. Chen, G.-H. Lee, Prof. S.-M. Peng
Department of Chemistry
National Taiwan University
Taipei 106 (Taiwan)
E-mail: kenwong@ntu.edu.tw

[**] The authors gratefully acknowledge the financial support from the National Science Council of Republic of China.

low-molecular-weight ruthenium complexes were reported to have an external quantum efficiency (*EQE*) of 1 %.[4] In 2000, LECs that used $[Ru(bpy)_3](ClO_4^-)_2$ (bpy: 2,2′-bipyridine) together with a gallium–indium eutectic electrode showed *EQE* values up to 1.8 %.[5] Later, $[Ru(bpy)_3]^{2+}(PF_6^-)_2$, blended with poly(methyl methacrylate) (PMMA), was reported to increase the *EQE* to 3 % as well as improve the film quality.[6] In 2002, a single-crystal LEC was made by repeatedly filling a nearly saturated solution of $[Ru(bpy)_3](ClO_4^-)_2$ between two indium tin oxide (ITO) slides, followed by evaporation of the solvent.[7] These devices possessed low turn-on voltages and exhibited an *EQE* of 3.4 %. Further performance improvements were achieved by reducing the self-quenching of excited states in $[Ru(bpy)_3]^{2+}$ through the addition of alkyl substituents on the bpy ligands,[8] raising the *EQE* to 4.8 % under dc bias and to 5.5 % under pulsed driving. Yet a further improvement based on $[Ru(bpy)_3](ClO_4^-)_2$ was achieved by forming a heterostructure device; moving the emission zone away from the electrode and giving an efficiency of 6.4 %.[9]

All ruthenium complexes described above gave only red-orange emission, because of their limited ligand-field splitting energies. To expand the emission colors of LECs, devices based on the yellow-emitting (560 nm) iridium complex $[Ir(ppy)_2(dtb\text{-}bpy)]PF_6$ (ppy: phenylpyridine; dtb-bpy: 4,4′-ditertbutyl-2,2′-bipyridine) were reported in 2004, exhibiting efficiencies of 5 % and 10 lm W^{-1}.[10,11] Replacement of the ppy ligands by F-mppy ligands (F-mppy: 2-(4′-fluorophenyl)-5-methylpyridine) resulted in green emission (531 nm) and an EL efficiency of 1.8 %.[11,12] On the other hand, the use of $dF(CF_3)ppy$ ligands ($dF(CF_3)ppy$: 2-(2,4-difluorophenyl)-5-trifluoromethylpyridine) increased the energy gap of the iridium complexes and shifted the EL emission to blue-green (500 nm, with an *EQE* of 0.75 %).[13] Another series of cationic phenylpyrazole-based iridium complexes were also recently reported to give blue (492 nm), green (542 nm), and red (635 nm) emission.[14] Blue, green, and red devices made of these complexes on ITO coated with poly(3,4-ethylenedioxythiophene)/poly(styrene sulfonate) (PEDOT/PSS) showed *EQE*s of 4.7, 6.9, and 7.4 %, respectively.

In general, the emissive layers of LECs are composed of neat films of emissive materials. In such a film, interactions between closely packed molecules usually lead to quenching of exited states, which is detrimental to the *EQE* values of the devices. Therefore, in addition to the tuning of emission colors, the capability of the ligands to provide steric hindrance to suppress self-quenching must also be carefully considered when designing ligands for emissive metal complexes. In our previous studies on oligofluorenes, we found that the introduction of aryl substituents on the tetrahedral C9 carbon atom of oligofluorenes can provide effective hindrance, suppressing interchromophore packing and self-quenching without perturbing the energy gaps of the molecules,[15–19] and thereby making the photoluminescence quantum yields (PLQYs) of oligo(9,9-diarylfluorene)s in neat films close to PLQY values in dilute solutions. Herein, we introduce 4,5-diaza-9,9′-spirobifluorene (sb)[20] as a steric and bulky auxiliary ligand for the cationic iridium complexes, $[Ir(ppy)_2sb]PF_6$ (**1**) and $[Ir(dFppy)_2sb]PF_6$ (**2**) (Scheme 1), and investigate the influence of the sb ligand on reducing the self-quenching. Comparative photophysical studies between **1** and **2** dispersed in a large-gap host and deposited as neat films reveal the advantageous ability of the sb ligand to retain the PLQY values of the complexes in neat films. As a result, these complexes can be used to make highly efficient single-layered, solid-state LECs, with EL efficiencies (7.1 %, 22.6 lm W^{-1} for **1**, 7.1 %, 26.2 lm W^{-1} for **2**) among the highest reported for orange-red (or yellow) and green solid-state LECs based on cationic transition-metal complexes. These results indicate that cationic transition-metal complexes with a high degree of steric hindrance are essential for highly efficient solid-state electrochemical cells.

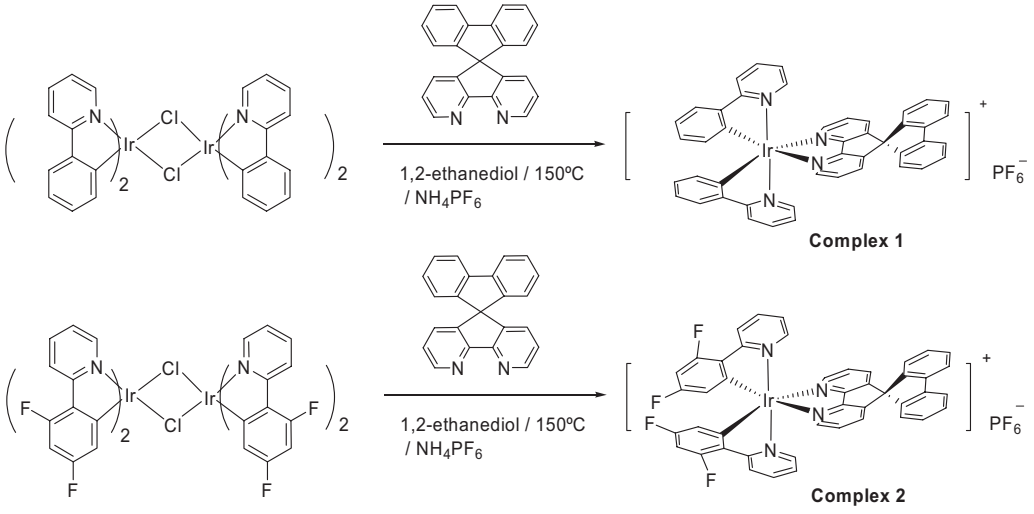

Scheme 1. Synthetic pathways and structures of complex **1** and complex **2**

2. Results and Discussion

2.1. Photophysical Properties

The synthesis of **1** and **2** is schematically shown in Scheme 1, and is described in detail in the Experimental section. The UV-vis absorption and PL spectra of complexes **1** and **2** in acetonitrile (MeCN) solutions (5×10^{-5} M) and as neat films (ca. 100 nm) are shown in Figure 1a and b, respectively. The observed absorption features in either solutions or films were similar for both complexes. The absorption spectra of these compounds shows intense bands (molar extinction coefficient $\varepsilon > 10^4$ $M^{-1}cm^{-1}$) in the ultraviolet part of the spectrum between 200 nm and 320 nm. These bands are associated with ligand-centered (LC) transitions of the ligands.[13,14] The LC bands are accompanied by weaker and broad bands (with molar extinction coefficients of ca. 1×10^3 to 5×10^3 $M^{-1}cm^{-1}$) that extend from 350 nm to slightly over 400 nm and are associated with both spin-allowed and spin-forbidden metal-to-ligand charge transfer (MLCT) transitions.[13,14] The high intensities of the MLCT bands in iridium-based complexes have been attributed to the effective mixing of these transitions with higher-lying spin-allowed transitions of the ligands.[13,14] The mixing is facilitated by the strong spin–orbit coupling of the Ir^{III} center. Solutions of **1** show orange-red PL, while those of **2** show green emission. The difference in emission color between **1** and **2** indicates that the introduction of the electron-withdrawing fluoro substituents on the ppy ligand has a strong effect on the energy levels of these complexes. It is also interesting to note that after replacing the dtb-bpy ligand with the sb ligand, the emission of complex **1** is red-shifted compared to the yellow emission of $Ir(ppy)_2(dtb\text{-}bpy)]PF_6$.[10] Room-temperature transient PL of complexes **1** and **2** in MeCN, as determined by the time-correlated single-photon counting technique (see the Experimental section for details) exhibits single-exponential decay behavior, and the fitted excited-state lifetimes for **1** and **2** are 0.33 and 0.39 μs, respectively (Table 1). Excited-state lifetimes on the order of microseconds are the signature of phosphorescence, which is associated with emission from the ^{3}MLCT states of the complexes that are formed by strong intersystem crossing, mediated by the iridium atom. The PLQYs of complexes **1** and **2** in MeCN, as determined with a calibrated integrating sphere (see the Experimental section for details), are 0.226 and 0.278, respectively (Table 1).

Spin-coated neat films of **1** and **2** exhibited PL spectra similar to those observed for their solutions (Fig. 1). However, these same films showed higher PLQY values and longer excited-state lifetimes (0.316, 0.60 μs for **1**, 0.31 0.59 μs for **2**, respectively) than MeCN solutions of the complexes (Table 1). Because MeCN is a strongly polar solvent and the emitters are ionic, the photophysical properties of complexes **1** and **2** could be significantly perturbed by strong solute–solvent interactions, strongly influencing the observed PLQYs and lifetimes of **1** and **2** in MeCN. This can be verified by measuring the photophysical properties of **1** and **2** in a less polar solvent (that still allows a high enough solubility for spectroscopic measurements), such as dichloromethane (DCM). In DCM (5×10^{-5} M), both **1** and **2** exhibited higher PLQYs and longer

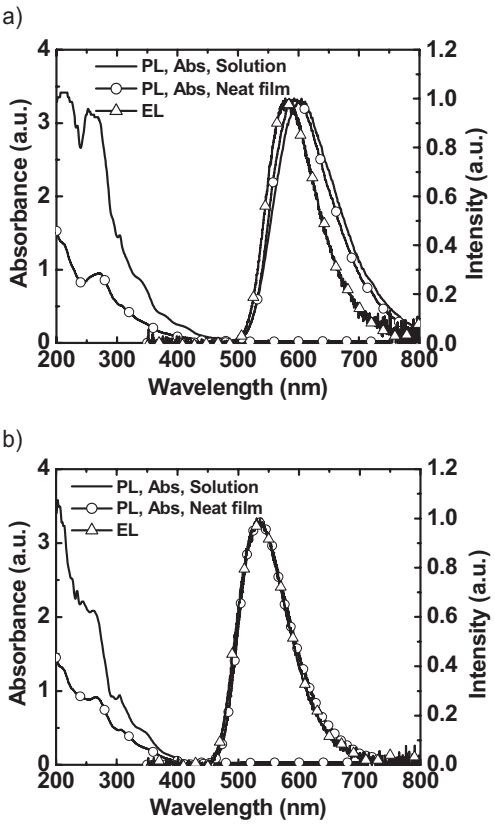

Figure 1. Absorption and PL spectra in acetonitrile (MeCN) solutions and in neat films of a) complex **1** and b) complex **2**. The EL spectra of complex **1** and complex **2** are also shown in (a) and (b), respectively.

Table 1. Summary of physical properties of complex **1** and complex **2**.

	$\lambda_{max,\ PL}$ [nm] [b]		PLQY, lifetime [μs] [c]		$E_{1/2}^{ox}$[V] [j]	$E_{1/2}^{red}$[V] [k]	$\Delta E_{1/2}$[V] [l]
	solution [a]	neat film	solution	film			
1	605	593	0.226, 0.33 [a] 0.467, 0.79 [d] –, 4.31 [e] –, 3.27 [f]	0.316, 0.60 [g] 0.667, 0.81 [h] 0.381, 0.72 [i]	1.35	–1.33	2.64
2	535	535	0.278, 0.39 [a] 0.364, 0.42 [d] –, 4.49 [e] –, 4.29 [f]	0.310, 0.59 [g] 0.421, 0.74 [h] 0.329, 0.55 [i]	1.70	–1.26	2.92

[a] Measured in MeCN (5×10^{-5} M) at room temperature. [b] PL peak wavelength. [c] Photoluminescence quantum yields and the excited-state lifetimes. [d] Measured in DCM (5×10^{-5} M) at room temperature. [e] Measured in MeCN (5×10^{-5} M) at 77 K. [f] Measured in DCM (5×10^{-5} M) at 77 K. [g] Neat films. [h] **1** and **2** were dispersed (1.5 mol%) in mCP films. [i] Films with 0.75 mole [$BMIM^+(PF6)^-$] per mole of **1** and **2**. [j] Oxidation potential. [k] Reduction potential. [l] The electrochemical gap $\Delta E_{1/2}$ is the difference between $E_{1/2}^{ox}$ and $E_{1/2}^{red}$, corrected by the potentials of the ferrocenium/ferrocene redox couple.

excited-state lifetimes (0.467, 0.79 μs for **1**, 0.364, 0.42 μs for **2**, respectively) than in MeCN (Table 1). Further suppression of the solute–solvent interactions and nonradiative deactivation processes by freezing either MeCN or DCM solutions of **1** and **2** to 77 K enhanced the excited-state lifetimes of complexes **1** and **2** to values beyond several microseconds (Table 1).

To better characterize the intrinsic photophysical properties of complexes **1** and **2** at room temperature the complexes were dispersed (1.5 mol %) in a large-gap, thin-film host of *m*-bis(*N*-carbazolyl)benzene (mCP), which is apolar and has a large triplet energy. The measured PLQY values and excited-state lifetimes of the dispersed mCP films are 0.667 and 0.81 μs for **1**, and 0.421 and 0.74 μs for **2** (Table 1). Thus, dilute dispersions of **1** and **2** in mCP exhibit higher PLQYs and longer excited-state lifetimes than neat films. Shorter lifetimes in neat films indicate that interactions between closely packed molecules provide additional relaxation pathways, lowering excited-state lifetimes and PLQYs. However, the PLQY values of **1** and **2** in neat films still remained at ca. 50 % and ca. 75 % of the PLQY values in mCP blend films. These retaining percentages for PLQYs in neat films are high compared to other phosphorescent molecules. For example, while $Ir(ppy)_3$ (1.5 mol % dispersed in 4,4′-bis(carbazol-9-yl)biphenyl, CBP) and bis[(4,6-difluorophenyl)pyridinato-*N*,C^2](picolinato)iridium(III) (FIrpic) (1.4 mol % dispersed in mCP) films had been reported to have very high PLQYs of (97 ± 2) % and (99 ± 1) %, respectively, the PLQY values of neat films $Ir(ppy)_3$ and FIrpic were only ca. 3 % and ca. 15 %, respectively.[21] Severe self-quenching in $Ir(ppy)_3$ and FIrpic implies that the ppy, dFppy, and picolinic acid ligands can not provide enough hindrance against intermolecular interactions in neat films. On the other hand, the high retaining percentages for neat-film PLQY values of complex **1** (with two ppy ligands and one sb ligand) and complex **2** (with two dFppy ligands and one sb ligand) compared to the PLQY values of dispersed films indicate that the sb ligands in these compounds provide effective steric hindrance, and greatly reduce self-quenching. It is worth noting that self-quenching in neat films of FIrpic is not as severe as that in neat films of $Ir(ppy)_3$. It is likely that the fluoro substituents on the ppy ligands hinder the intermolecular interactions.[21] Here, a similar effect is also observed for complex **2**, which exhibits a higher PLQY retaining percentage (74 %) than complex **1**.

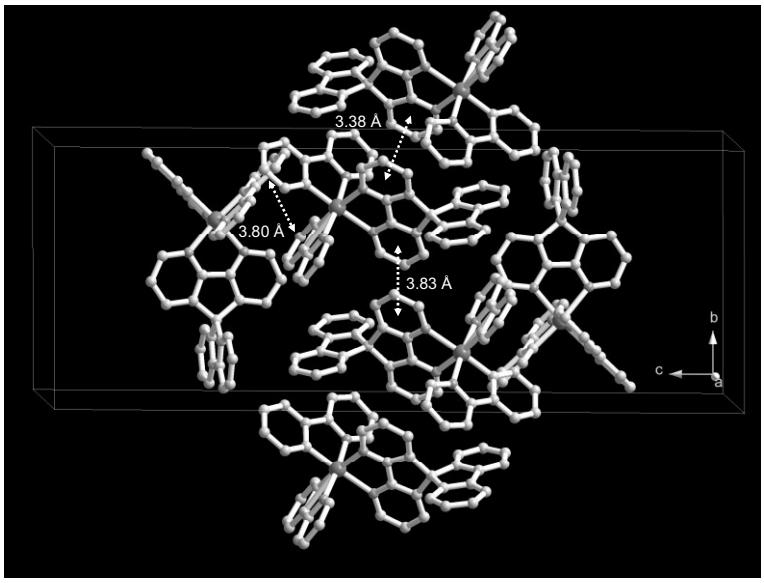

Figure 2. Crystal packing of complex **1** in a unit cell. The solvent molecules, counter anions (PF_6^-), and hydrogen atoms are omitted for clarity.

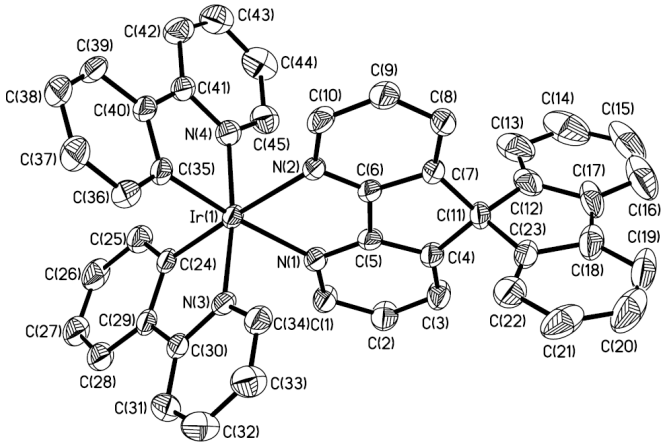

Figure 3. The molecular structure of complex **1**. Thermal ellipsoids are drawn at 50 % probability.

2.2. Crystal Structure

Crystals of **1** suitable for the X-ray diffraction analysis were obtained by slow evaporation from a diethyl ether solution. Complex **1** was packed in a monoclinic crystal structure with space group *P*2/c (Fig. 2). As depicted in Figure 3, complex **1** with two cyclometalated 2-phenylpyridine (*C*^*N*) ligands and one 4,5-diaza-9,9′-spirobifluorene (*N*^*N*) ligand exhibited a distorted octahedral geometry around the Ir center. This was indicated by the small bite angles of C(35)–Ir(1)–N(4) (80.7° ±0.2°), C(24)–Ir(1)–N(3) (80.23° ± 0.18°), N(1)–Ir(1)–N(2) (80.00° ± 0.14°), and twisted bond angles of N(4)–Ir(1)–N(3) (172.29° ± 0.16°), C(35)–Ir(1)–N(1) (173.93° ± 0.17°), C(24)–Ir(1)–N(2) (175.96° ± 0.17°). The Ir–N bond distances between the Ir center and 4,5-diaza-9,9′-spirobifluorene, Ir(1)–N(1) (2.203 ±0.004) Å and Ir(1)–N(2) (2.211 ±0.004) Å are significantly longer than those between the Ir center and 2-phenylpyridine, Ir(1)–N(0) (2.050 ± 0.004) Å and Ir(1)–N(4) (2.036 ± 0.004) Å. This is attributable to the anionic nature of the cyclometalated 2-phenylpyridine ligands, which have a stronger interaction with the cationic Ir^{III} ion. By carefully inspecting the crystal packing in a unit cell (Fig. 2), we found that the bulkiness of 4,5-diaza-9,9′-spirobifluorene ligand plays an important role in preventing intermolecular interactions, as in-

dicated by the closest Ir-to-Ir distance of 9.21 Å along the *b*-axis and 8.62 Å along the *c*-axis (Fig. 2). Some plane-to-plane packing motifs between coplanar chelating ligands were found. The closest plane-to-plane distances between the edges of diazafluorene subunits of two neighboring complexes along the *b*-axis were calculated as ca. 3.38 Å and 3.83 Å. Along the *c*-axis, the phenylene rings of the 2-phenylpyridine ligands of neighboring molecules were also found to have a twisted face-to-face arrangement, with a plane-to-plane distance of ca. 3.80 Å. On one hand, this plane-to-plane overlapping is small (along the edge and twisted); on the other hand, the distance is relatively large, rendering the intermolecular π–π interactions relatively weak.

2.3. Electrochemical Properties

Figure 4 depicts the electrochemical characteristics of complex **1** and complex **2** probed by cyclic voltammetry (CV, see the Experimental section for details), and the measured redox

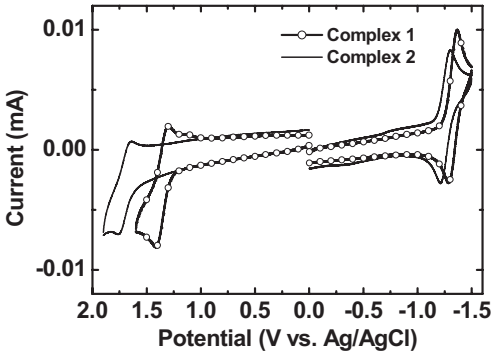

Figure 4. Cyclic voltammograms of complex **1** and complex **2**. Potentials were recorded versus a Ag/AgCl reference electrode (saturated).

potentials are listed in Table 1. Complex **2** exhibits a reversible oxidation peak at 1.70 V versus Ag/AgCl, which is significantly higher than that of complex **1** (1.35 V). The highest occupied molecular orbital (HOMO) of $[Ir(ppy)_2(dtb\text{-}bpy)]PF_6$ has been reported to be a mixture of the d orbitals of iridium and the π orbitals of the phenyl ring of the ppy ligand.[13] Because **1** and **2** are also cationic ppy-based Ir^{III} complexes, their HOMO distributions should be similar to that of $[Ir(ppy)_2(dtb\text{-}bpy)]PF_6$. The higher oxidation potential of complex **2** compared to that of complex **1** indicates that the two electron-withdrawing fluoro substituents on the phenyl ring of the ppy ligand possibly reduce the electron density on the Ir metal center, and consequently stabilize the HOMO level. According to previous studies, the lowest unoccupied molecular orbital (LUMO) of $[Ir(ppy)_2(dtb\text{-}bpy)]PF_6$ is located mainly on the dtb-bpy ligand,[13] and therefore, for complex **1** and complex **2**, reduction is expected to take place on the auxiliary sb ligand. The similar reduction potentials of complex **1** (–1.33 V) and complex **2** (–1.26 V) confirm that this mutual ligand is responsible for the reduction of both compounds. The reduction potential of complex **2** is slightly smaller than that of complex **1**, possibly because the fluoro substituents make complex **2** more electrophilic and thus easier to reduce.[13] With the HOMO level significantly shifted, and the LUMO level only slightly changed as a result of fluoro substitution, the PL emission of complex **2** is significantly blue-shifted compared to the PL emission of complex **1**. This behavior, where energy gaps can be tuned through the introduction of substituents with different electronic properties on the ppy ligands, is characteristic of Ir complexes.

2.4. Electroluminescent Properties

In the operation of LEC devices, a delayed EL response is typically observed when a constant bias voltage is applied. This delayed response is associated with the time needed for counterions in the LECs to redistribute under the applied bias. For the cases of neat films of complexes **1** and **2**, the redistribution of the anions (PF_6^-) leads to the formation of a region of Ir^{IV}/Ir^{III} complexes (p-type) near the anode and a region of Ir^{III}/Ir^{II} complexes (n-type) near the cathode.[22] With the formation of p- and n-type regions near the electrodes, carrier injection is enhanced, leading to a gradually increasing device current and emission intensity. Devices based on neat films of complex **1** and complex **2** (with the following structure: glass substrate/ITO/complex **1** or **2** (100 nm)/Ag) exhibited very long response times. Very slow device response times (e.g., tens of hours to reach the maximum brightness) have also been observed before for other LEC materials (e.g., $[Ru(bpy)_3](PF_6)_2$ derivatives with esterified ligands).[4] Possibly, bulky side groups on molecules impede the migration of ions. Thus, to accelerate the formation of the p- and n-doped regions in the emissive layer, 0.75 mol of the ionic liquid 1-butyl-3-methylimidazolium hexafluorophosphate $[BMIM^+(PF_6)^-]$ per mole of complex **1** or complex **2** was added to provide additional PF_6^- anions.[23]

In polymer LECs, it has been reported that incorporation of polar salts into conjugated polymer films might induce aggregates or phase separation as a result of discrepancies in polarity.[24–26] To study the effect of the addition of $[BMIM^+(PF_6)^-]$ on thin-film morphologies of complexes **1** and **2**, atomic force microscopy (AFM) measurements of thin films were performed. As shown in Figure 5, AFM images for films of complexes **1** and **2** with and without $[BMIM^+(PF_6)^-]$ coated on ITO glass substrates showed no significant differences, and all give a similar root-mean-square (RMS) roughnesses of ca. 1 nm. At this concentration of $[BMIM^+(PF_6)^-]$ in complex **1** or complex **2** (molar ratio 0.75:1), no particular aggregation features or phase separation were observed, and uniform spin-coated thin films could be routinely obtained. These characteristics are possibly associated with the ionic nature of complexes **1** and **2**, which may make them more compatible with the added salts. Furthermore, to examine the effects of the $[BMIM^+(PF_6)^-]$ addition on the photophysical properties of complexes **1** and **2**, the PLQY values and excited-state lifetimes of the blend films were also measured, and are shown in Table 1. In general, films of both **1** and **2** containing $[BMIM^+(PF_6)^-]$ (molar ratio 1:0.75) exhibited PLQYs and excited-state lifetimes compar-

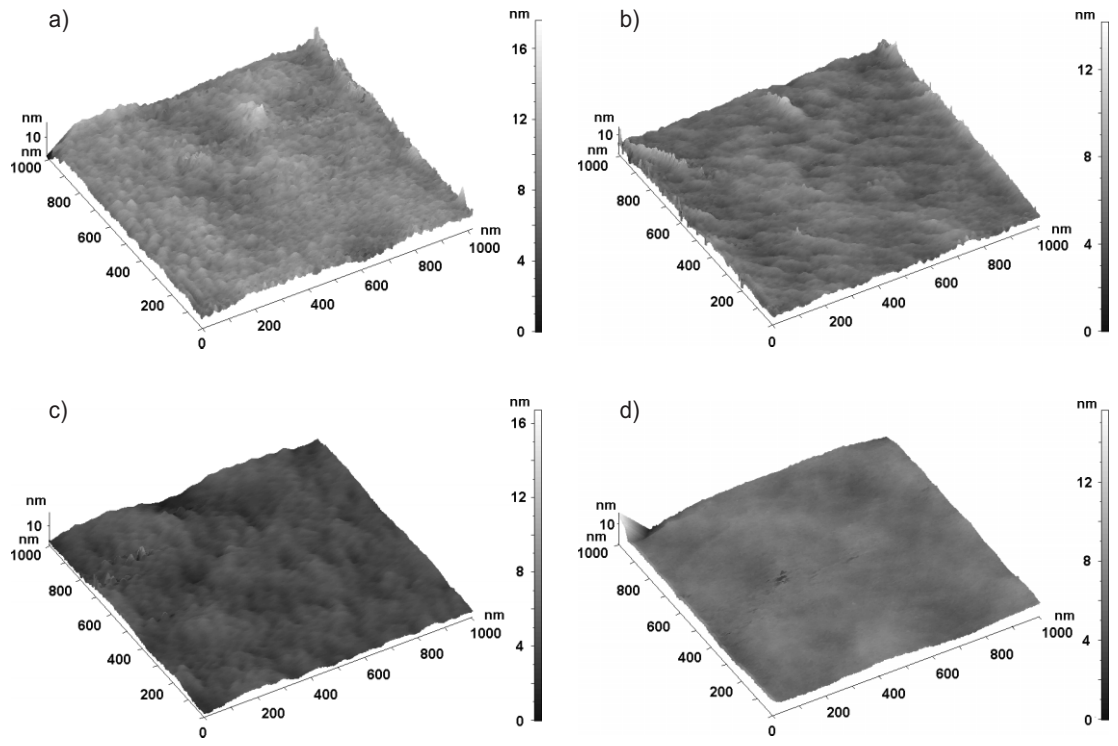

Figure 5. 3D AFM images of a) a neat film of complex **1**, b) a blend film of [$BMIM^+(PF_6)^-$] and complex **1** (molar ratio 0.75:1), c) a neat film of complex **2**, and d) a blend film of [$BMIM^+(PF_6)^-$] and complex **2** (molar ratio 0.75:1).

able to those of neat films, indicating that the addition of [$BMIM^+(PF_6)^-$] does not induce particular emission quenching. Stable operation was also achieved in devices using such a formulation. The characteristics of these devices (structure: glass substrate/ITO/**1**:[$BMIM^+(PF_6)^-$] or **2**:[$BMIM^+(PF_6)^-$] (100 nm)/Ag) are discussed below, and are summarized in Table 2.

Table 2. Summary of the LEC device characteristics based on complex **1** and complex **2**.

		$\lambda_{max,\ EL}$ [a] [nm]	t_{max} [b] [min]	L_{max} [c] [cd cm^{-2}]	$\eta_{ext,\ max}$, $\eta_{p,\ max}$ [d] [%, lm W^{-1}]	Lifetime [e] [h]
1	(2.6 V)	580	170	330	6.2, 19.0	26
	(2.5 V)		150	100	7.1, 22.6	54
2	(2.9 V)	535	85	145	6.6, 23.6	6.7
	(2.8 V)		90	52	7.1, 26.2	12

[a] EL peak wavelength. [b] Time required to reach the maximal brightness. [c] Maximal brightness achieved at a constant bias voltage. [d] Maximal external quantum efficiency and maximal power efficiency achieved at a constant bias voltage. [e] The time for the brightness of the device to decay from the maximum to half of the maximum under a constant bias voltage.

A distinct characteristic of LECs is that they can be operated at a bias voltage close to E_g/e. As shown in Table 1, the electrochemical gaps ($\Delta E_{1/2}$) for complex **1** and complex **2** are 2.64 and 2.92 eV, respectively. The devices based on complex **1** and complex **2** were thus first tested under the biases of 2.6 V and 2.9 V, respectively, even though the energy gaps in films are usually smaller than those in solutions because of environmental polarization. EL spectra of the devices based on complex **1** and complex **2** (with added [$BMIM^+(PF_6)^-$]) are shown in Figure 1a and b, respectively, to allow comparison with their PL spectra. EL spectra are basically similar to PL spectra, indicating similar emission mechanisms. The Commission Internationale de L'Éclairage (CIE) coordinates for the EL spectra of complex **1** and complex **2** are (0.51,0.48) and (0.35,0.57), respectively. Time-dependent brightnesses and current densities of the devices operated under the bias conditions described above are shown in Figure 6a and b for complex **1** and complex **2**, respectively. Both devices exhibited similar electrical characteristics. After the bias was applied, the currents of both devices first increased with time, and then stayed at a constant level after 350–400 minutes. On the other hand, the brightness first increased with the current and reached a maximum of 330 cd m^{-2} for complex **1** at ca. 170 minutes and of 145 cd m^{-2} for complex **2** at ca. 85 minutes. The brightness then decreased with time, even though the device current remained constant. The decrease in brightness was irreversible, i.e., the maximum brightness obtained in the first measurement could not be fully recovered in subsequent measurements, even under the same driving conditions. This is rationally associated with the degradation of the emissive material during the LEC operation, which is commonly seen in LEC devices.[27]

The lifetime of the devices, defined as the time it takes for the brightness of the device to decay half-maximum under a constant bias (2.6 V for complex **1** and 2.9 V for complex **2**),

ADVANCED FUNCTIONAL MATERIALS

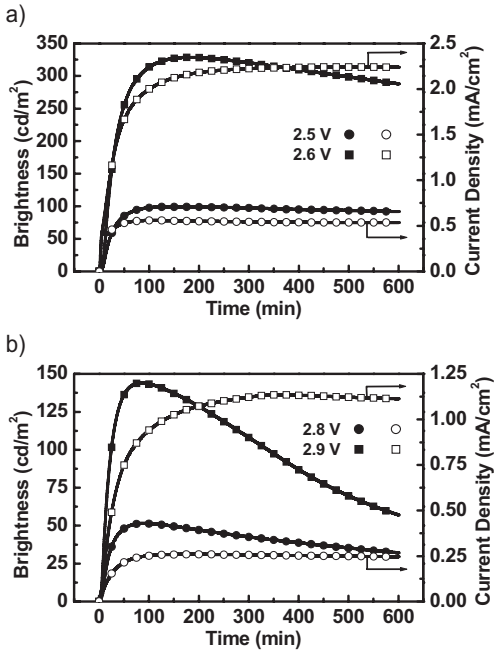

Figure 6. Time-dependent brightness and current–density diagrams of the single-layered LEC device for a) complex **1** driven at 2.6 or 2.5 V, and b) complex **2** driven at 2.9 or 2.8 V.

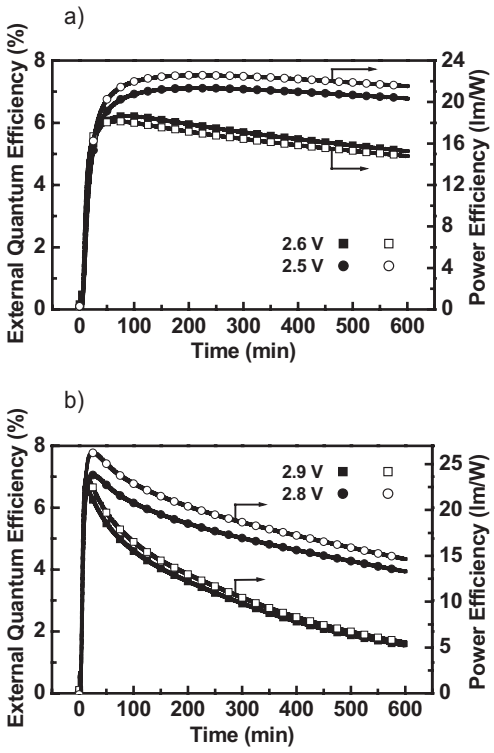

Figure 7. The time-dependent *EQE* and the corresponding power efficiency of the single-layered LEC device for a) complex **1** driven at 2.6 or 2.5 V, and b) complex **2** driven at 2.9 or 2.8 V.

was ca. 26 h (**1**, extrapolated) and 6.7 h (**2**), respectively. Although operated at a lower current density, the lifetime of the device based on complex **2** is significantly shorter than that of the device based on complex **1**. Irreversible multiple oxidation and subsequent decomposition under a high electric field have been proposed as mechanisms for degradation of LECs based on cationic iridium complexes.[23,28] Because a higher bias voltage is required for operating the device based on complex **2** because of its larger energy gap, the higher electric field in the emissive layer of the complex **2** device perhaps accelerated the degradation. To mitigate the device degradation, slightly lower bias voltages of 2.5 and 2.8 V were applied for testing the devices based on complex **1** and complex **2**, respectively. As shown in Figure 6a and b, a slight reduction of the applied bias by 0.1 V led to greatly reduced brightness degradation rates for both devices. The lifetimes of the device based on complex **1**, at a bias of 2.5 V, driving and the device based on complex **2**, at 2.8 V, are ca. 54 and ca. 12 h (both extrapolated), respectively, roughly two times longer than those driven at 0.1 V higher bias voltages. The longer device lifetimes, however, are achieved at the expense of brightness. Therefore, emissive materials with high quantum yields are essential for the operation of LECs at a practical brightness at the lowest possible bias, which would ensure long lifetime operation of LECs.

Time-dependent *EQE*s and corresponding power efficiencies of the device based on complex **1** at a 2.6 V bias and the device based on complex **2** at a 2.9 V bias are shown in Figure 7a and b, respectively. The time evolution of the *EQE* was similar for both devices. Very shortly after the forward bias was applied, the *EQE* was low because of unbalanced carrier injection. During the formation of the p- and n-type regions near the electrodes, the carrier-injection balance improved, and the *EQE* of the devices increased rapidly. The peak *EQE* and the peak power efficiency were 6.2 % and 19.0 lm W^{-1}, respectively, for the complex **1** device at a bias of 2.6 V, and 6.6 %, and 23.6 lm W^{-1}, respectively, for the complex **2** device at a bias of 2.9 V. It should be noted that the peak efficiencies occurred before the currents reached their final maximal values. This phenomenon can be associated with two factors. Firstly, although both contacts are becoming more ohmic and the carrier injection at both electrodes becomes more balanced with the formation of the p- and n-type regions near the electrodes, the carrier-recombination zone may move towards one of the electrodes because of differences between electron and hole mobilities. The relocation of the recombination zone to the vicinity of an electrode may cause exciton quenching, such that the *EQE* of the device decreases with time while the current and the brightness are still increasing. Secondly, degradation of the emissive material under a high field also contributes to the decrease of the *EQE* when the recombination zone is still moving, or when the recombination zone is fixed.

When driven under biases 0.1 V lower, both LEC devices exhibited higher peak *EQE* values and lower degradation rates. As shown in Figure 7a and b, the peak *EQE* and the peak power efficiency are 7.1 % and 22.6 lm W^{-1}, respectively, for the complex **1** device at a bias of 2.5 V, and 7.1 % and 26.2 lm W^{-1}, respectively, for the complex **2** device at a bias of 2.8 V. It is in-

teresting to note that the peak *EQE*s of the single-layered devices (no PEDOT/PSS was used) based on complex **1** and complex **2** approximately approach the upper limits that one would expect from the PLQYs of their neat films, when considering an optical out-coupling efficiency of ca. 20 % from a typical layered light-emitting device structure. To our knowledge, these *EQE*s are among the highest values reported for orange-red (or yellow) and green solid-state LECs based on cationic transition-metal complexes. These results indicate that cationic transition-metal complexes with superior steric hindrance are essential and useful for achieving highly efficient solid-state LECs.

3. Conclusion

We have reported the syntheses and characterization of two novel cationic iridium complexes, $[Ir(ppy)_2sb]PF_6$ (complex **1**) and $[Ir(dFppy)_2sb]PF_6$ (complex **2**), for solid-state light-emitting electrochemical cells. Complex **1** and complex **2** exhibit efficient orange-red and green emission, respectively, both in solutions and in neat films. Both complexes retain rather high percentages of their PLQYs in neat films when compared with the PLQYs of both complexes dispersed in a solid-state mCP host. The highly retained PLQY values in neat films suggest effective steric hindrance provided by the diazaspirobifluorene-based (sb) ligands. CV measurements of both complexes indicate that fluoro substituents on the phenyl ring of the ppy ligand cause the lowering of the HOMO level and the blue-shifted emission of complex **2**. The devices using single-layered neat films of $[Ir(ppy)_2sb]PF_6^-$ and $[Ir(dFppy)_2sb]PF_6^-$ achieve high peak external quantum efficiencies and power efficiencies of 7.1 % and 22.6 lm W^{-1} at 2.5 V (complex **1**), and 7.1 % and 26.2 lm W^{-1} at 2.8 V (complex **2**). These efficiencies are among the highest reported for solid-state light-emitting electrochemical cells, and indicate that the cationic transition metal complexes containing ligands with good steric hindrance (e.g., diazaspirobifluorene-based ligands reported here) are excellent candidates for highly efficient solid-state electrochemical cells.

4. Experimental

General Experiments: ^{1}H NMR and ^{13}C NMR spectra of compounds were collected on a 400 MHz spectrometer at room temperature. Photophysical characteristics of complexes **1** and **2** in solution were collected at room temperature by using 5×10^{-5} M MeCN solutions, which were carefully purged with nitrogen prior to measurements. Neat and mCP-blended films of complex **1** and **2** were spin-coated onto quartz substrates from the MeCN and DCM solutions, respectively. The thickness of the spin-coated films was ca. 100 nm, as measured by ellipsometry. UV-vis absorption spectra were recorded on a spectrophotometer. PL spectra were measured with a cooled charge-coupled device (CCD), connected to a monochromator using the 325 nm line of the He–Cd laser as the excitation. PLQYs for solution and thin-film samples were both determined with a calibrated integrating sphere system. Excited-state lifetimes of samples were measured using the time-correlated single-photon counting technique, in which a photomultiplier and a sub-nanosecond pulsed UV laser diode were used as the detector and the pulsed excitation source and the PL signals were detected at the peak PL wavelengths. Oxidation and reduction potentials of complexes **1** and **2** were determined by cyclic voltammetry (scan rate 100 mV s^{-1}) in MeCN solutions (1.0 mM). A glassy carbon electrode and a platinum wire were used as the working electrode and the counter electrode, respectively. All potentials were recorded versus the Ag/AgCl (saturated) reference electrode. Oxidation CV was performed using 0.1 M of tetra-*n*-butylammonium hexafluorophosphate ($TBAPF_6$) as the supporting electrolyte. The ferrocenium/ferrocene redox couple in MeCN/$TBAPF_6$ showed $E^{0\prime} = +0.47$ V versus Ag/AgCl (saturated). For reduction CV, 0.1 M of tetra-*n*-butylammonium perchlorate (TBAP) in MeCN was used as the supporting electrolyte. The ferrocenium/ferrocene redox couple in MeCN/TBAP showed $E^{0\prime} = +0.43$ V versus Ag/AgCl (saturated). AFM images of films of complexes **1** and **2** with and without $[BMIM^+(PF_6)^-]$ spin-coated onto ITO glass substrates were obtained by using a scanning probe microscope in tapping mode.

Synthesis of $[Ir(ppy)_2sb]PF_6$: The complex was synthesized as shown in Scheme 1, by adapting a literature procedure [29–31]. A mixture of bis-(μ)-chlorotetrakis(2-phenyl)-pyridinato-C^2,N)diiridium(III) (1.0 mmol, 0.7 g) and 4,5-diaza-9,9′-spirobifluorene (2.2 mmol, 0.7 g) was dissolved in 1,2-ethanediol (20 mL) under argon, and the solution was kept at 150 °C for 12 h. After 12 h, the solution was cooled to room temperature, and an aqueous solution of NH_4PF_6 (10 g in 100 mL deionized water) was added to the reaction mixture, producing a yellow suspension. The solution was then cooled to 5 °C for 1 h, and was filtered. The collected solid was dried in an oven (80 °C). Subsequent column chromatography on silica gel (CH_2Cl_2/MeCN = 10:1) afforded a bright orange powder (1.24 g, 76 %). IR (KBr) ν 417, 557, 733, 758, 841, 1119, 1164, 1228, 1268, 1413, 1478, 1583, 1608 cm^{-1}; ^{1}H NMR (400 MHz, d_6-acetone, δ): 8.29 (4H, t, J = 8.4 Hz), 8.20 (2H, d, J = 7.2 Hz), 8.05 (2H, td, J = 8.0 and 1.6 Hz), 7.92 (2H, dd, J = 8.0, 1.2 Hz), 7.89 (2H, dd, J = 8.0, 2.0 Hz), 7.65–7.60 (m, 4H), 7.55 (2H, td, J = 8.0 and 1.2 Hz), 7.36 (2H, td, J = 8.0 and 1.6 Hz), 7.26 (2H, td, J = 8.0 and 1.2 Hz), 7.06 (2H, td, J = 8.0 and 1.2 Hz), 6.96 (2H, td, J = 8.0 and 1.6 Hz), 6.89 (2H, d, J = 7.6 Hz), 6.51 (2H, d, J = 8.0 Hz); ^{13}C NMR (100 MHz, d_6-acetone, δ): 168.4, 162.8, 150.7, 149.6, 145.4, 145.3, 144.3, 142.9, 142.8, 139.6, 135.4, 132.6, 130.8, 130.3, 129.3, 129.2, 125.4, 124.7, 124.6, 123.5, 121.9, 120.6. Mass spectrometry (MS) (m/z, FAB$^+$) 289 (35), 307 (65), 499 (40), 501 (60), 817 (60), 819 (100); High-resolution MS (HRMS) (m/z, FAB$^+$) calcd for $C_{45}H_{30}IrN_4$, 819.2100; found, 819.2100.

Synthesis of $[Ir(dFppy)_2sb]PF_6$: Similar to the procedures described above for the synthesis of $[Ir(ppy)_2sb]PF_6$ (Scheme 1), bis-μ-chlorotetrakis(2-(4,6-difluorophenyl)-pyridinato-C^2,N)diiridium(III) (1.0 mmol, 1.2 g) reacted with 4,5-diaza-9,9′-spirobifluorene (2.2 mmol, 0.7 g) in 1,2-ethanediol (20 mL) gave a yellow suspension. Column chromatography on silica gel (CH_2Cl_2/MeCN = 10:1) afforded a bright yellow powder (0.83 g, 81 %). IR (KBr) ν 440, 561, 733, 762, 841, 985, 1106, 1124, 1168, 1243, 1297, 1412, 1476, 1573, 1598 cm^{-1}; ^{1}H NMR (400 Mhz, d_6-acetone, δ) 8.44 (2H, d, J = 8.0 Hz), 8.37 (2H, d, J = 5.2 Hz), 8.15 (2H, t, J = 8.0 Hz), 8.11–8.08 (m, 4H), 7.70–7.63 (m, 4H), 7.55 (4H, t, J = 8.0 Hz), 7.47–7.44 (m, 2H), 7.26 (2H, J = 7.6 Hz), 6.90 (2H, d, J = 7.6 Hz), 6.81 (2H, td, J = 9.4 and 2.4 Hz), 5.96 (2H, dd, J = 8.6 and 2.0 Hz); ^{13}C NMR (100 Mhz, d_6-acetone, δ): 169.4, 169.3, 168.8, 178.7, 167.3, 167.1, 166.9, 166.8, 164.7, 164.6, 155.6, 155.4, 154.3, 153.7, 153.6, 148.8, 147.2, 146.9, 145.1, 140.4, 140.3, 140.2, 134.7, 134.6, 134.0, 133.9, 133.6, 129.7, 129.6, 129.0, 128.6, 126.2, 119.3, 119.1, 104.2, 104.0, 103.8, 72.3, 34.8, 34.7,34.6, 34.5, 34.4, 34.2, 34.1, 33.9, 33.7. MS (m/z, FAB$^+$) 307 (85), 573 (50), 891 (90); HRMS (m/z, FAB$^+$) calcd for $C_{45}H_{26}F_4IrN_4$, 891.1723; found, 891.1743.

Fabrication and Characterization of LEC Devices: ITO-coated glass substrates were cleaned and treated with UV/ozone prior to coating of the emissive layer. The preparation of solutions of **1** and **2** and spin-coating of neat films (ca. 100 nm) of **1** and **2** were performed in the nitrogen atmosphere of a glove-box. To reduce the turn-on time of the LEC device, 0.75 mol of the ionic liquid $[BMIM^+PF_6^-]$ per mole of complex **1** (or complex **2**) was added to enhance the ionic conductivity of the thin films [23]. After spin coating, the neat films were then baked at 70 °C for 15 h, followed by thermal evaporation of a 150 nm Ag top contact in a vacuum chamber (ca. 10^{-6} Torr, 1 Torr = 1.333×10^2 Pa). The electrical and emission characteristics of LEC devices were mea-

ADVANCED FUNCTIONAL MATERIALS

sured using a source-measurement unit and a Si photodiode calibrated with a Photo Research PR-650 spectroradiometer. All device measurements were performed under a constant bias voltage (2.6 or 2.5 V for complex **1**, 2.9 or 2.8 V for complex **2**). The EL spectra were taken with a calibrated CCD spectrograph.

Received: April 25, 2006
Revised: May 25, 2006
Published online: February 1, 2007

[1] Q. Pei, G. Yu, C. Zhang, Y. Yang, A. J. Heeger, *Science* **1995**, *269*, 1086.
[2] J. Slinker, D. Bernards, P. L. Houston, H. D. Abruña, S. Bernhard, G. G. Malliaras, *Chem. Commun.* **2003**, 2392.
[3] J. K. Lee, D. S. Yoo, E. S. Handy, M. F. Rubner, *Appl. Phys. Lett.* **1996**, *69*, 1686.
[4] E. S. Handy, A. J. Pal, M. F. Rubner, *J. Am. Chem. Soc.* **1999**, *121*, 3525.
[5] F. G. Gao, A. J. Bard, *J. Am. Chem. Soc.* **2000**, *122*, 7426.
[6] H. Rudmann, M. F. Rubner, *J. Appl. Phys.* **2001**, *90*, 4338.
[7] C. Y. Liu, A. J. Bard, *J. Am. Chem. Soc.* **2002**, *124*, 4190.
[8] H. Rudmann, S. Shimada, M. F. Rubner, *J. Am. Chem. Soc.* **2002**, *124*, 4918.
[9] C. Y. Liu, A. J. Bard, *Appl. Phys. Lett.* **2005**, *87*, 061 110.
[10] J. D. Slinker, A. A. Gorodetsky, M. S. Lowry, J. Wang, S. Parker, R. Rohl, S. Bernhard, G. G. Malliaras, *J. Am. Chem. Soc.* **2004**, *126*, 2763.
[11] M. S. Lowry, W. R. Hudson, R. A. Pascal, Jr., S. Bernhard, *J. Am. Chem. Soc.* **2004**, *126*, 14 129.
[12] J. D. Slinker, C. Y. Koh, G. G. Malliaras, M. S. Lowry, S. Bernhard, *Appl. Phys. Lett.* **2005**, *86*, 173 506.
[13] M. S. Lowry, J. I. Goldsmith, J. D. Slinker, R. Rohl, R. A. Pascal, Jr., G. G. Malliaras, S. Bernhard, *Chem. Mater.* **2005**, *17*, 5712.
[14] A. B. Tamayo, S. Garon, T. Sajoto, P. I. Djurovich, I. M. Tsyba, R. Bau, M. E. Thompson, *Inorg. Chem.* **2005**, *44*, 8723.
[15] C. C. Wu, Y. T. Lin, H. H. Chiang, T. Y. Cho, C. W. Chen, K. T. Wong, Y. L. Liao, G. H. Lee, S. M. Peng, *Appl. Phys. Lett.* **2002**, *81*, 577.
[16] K. T. Wong, Y. Y. Chien, R. T. Chen, C. F. Wang, Y. T. Lin, H. H. Chiang, P. Y. Hsieh, C. C. Wu, C. H. Chou, Y. O. Su, G. H. Lee, S. M. Peng, *J. Am. Chem. Soc.* **2002**, *124*, 11 576.
[17] C. C. Wu, T. L. Liu, W. Y. Hung, Y. T. Lin, K. T. Wong, R. T. Chen, Y. M. Chen, Y. Y. Chien, *J. Am. Chem. Soc.* **2003**, *125*, 3710.
[18] C. C. Wu, Y. T. Lin, K. T. Wong, R. T. Chen, Y. Y. Chien, *Adv. Mater.* **2004**, *16*, 61.
[19] T. C. Chao, Y. T. Lin, C. Y. Yang, T. S. Hung, H. C. Chou, C. C. Wu, K. T. Wong, *Adv. Mater.* **2005**, *17*, 992.
[20] K. T. Wong, R. T. Chen, F. C. Fang, C. C. Wu, Y. T. Lin, *Org. Lett.* **2005**, *7*, 1979.
[21] Y. Kawamura, K. Goushi, J. Brooks, J. J. Brown, H. Sasabe, C. Adachi, *Appl. Phys. Lett.* **2005**, *86*, 071 104.
[22] H. Rudmann, S. Shimada, M. F. Rubner, *J. Appl. Phys.* **2003**, *94*, 115.
[23] S. T. Parker, J. D. Slinker, M. S. Lowry, M. P. Cox, S. Bernhard, G. G. Malliaras, *Chem. Mater.* **2005**, *17*, 3187.
[24] C. Yang, Q. Sun, J. Qiao, Y. Li, *J. Phys. Chem. B* **2003**, *107*, 12 981.
[25] L. Edman, M. Pauchard, D. Moses, A. J. Heeger, *J. Appl. Phys.* **2004**, *95*, 4357.
[26] F. P. Wenzl, P. Pachler, C. Suess, A. Haase, E. J. W. List, P. Poelt, D. Somitsch, P. Knoll, U. Scherf, G. Leising, *Adv. Funct. Mater.* **2004**, *14*, 441.
[27] G. Kalyuzhny, M. Buda, J. McNeill, P. Barbara, A. J. Bard, *J. Am. Chem. Soc.* **2003**, *125*, 6272.
[28] Y. Ohsawa, S. Sprouse, K. A. King, M. K. DeArmond, K. W. Hanck, R. J. Watts, *J. Phys. Chem.* **1987**, *91*, 1047.
[29] S. Sprouse, K. A. King, P. J. Spellane, R. J. Watts, *J. Am. Chem. Soc.* **1984**, *106*, 6647.
[30] O. Lohse, P. Thevenin, E. Waldvogel, *Synlett* **1999**, 45.
[31] M. Nonoyama, *Bull. Chem. Soc. Jpn.* **1974**, *47*, 767.